Science and Technology Indonesia
e-ISSN:2580-4391 p-ISSN:2580-4405
Vol. 11, No. 4, October 2026

Research Paper

Semi-Analytical and Numerical Solutions of the KdV-BBM Equation Using Differential Transformation Method and iRK-5 Based Method of Lines

Dita Ardiana[1], Ummu Habibah[1*], Arnida Lailatul Latifah[2], Trisilowati[1]

[1]Department of Mathematics, Brawijaya University, Malang, East Java, 100190, Indonesia
[2]Research Center for Computing, National Research and Innovation Agency, Jl. Raya Jakarta-Bogor KM 46, Bogor, West Java, 16911, Indonesia
*Corresponding author: ummu_habibah@ub.ac.id

Abstract
The Korteweg-de Vries-Benjamin-Bona-Mahony (KdV-BBM) equation is a fundamental mathematical model describing nonlinear long-wave propagation in dispersive media. This study presents a comprehensive computational investigation employing two distinct and complementary approaches: a tailored semi-analytical Differential Transformation Method (DTM) and a numerical Method of Lines (MOL) coupled with an improved fifth-order Runge-Kutta (iRK-5) scheme to solve both homogeneous and inhomogeneous KdV-BBM equations. The scientific novelty of this work lies in optimizing these two independent frameworks to achieve high accuracy without requiring restrictive linearization or excessively small time steps. Semi-analytically, DTM is optimized using prescribed Cauchy boundary conditions for the homogeneous model to supply essential derivative data that guarantees coefficient uniqueness and accelerates series convergence, while Nayar's Theorem is incorporated to efficiently circumvent complex recurrence relations in the inhomogeneous case via variable separability. Numerically, the continuous PDE is discretized spatially via centered differences and integrated in time using the high-order iRK-5 scheme. Both approaches demonstrate exceptional performance in resolving the KdV-BBM model. Comparative evaluations demonstrate that the MOL(iRK-5) scheme superiorly preserves physical wave integrity, soliton peak height, and phase characteristics over extended simulation periods (T = 30), significantly outperforming standard explicit Fourth-Order Runge-Kutta (RK-4) and implicit Crank-Nicolson (C-N) methods. Unlike lower-order implicit schemes like C-N, which exhibit limited temporal accuracy ($O(\Delta t^2)$) and high matrix inversion costs, or RK-4 which faces severe CFL constraints, iRK-5 achieves higher temporal precision ($O(\Delta t^5)$) and an expanded stability domain, allowing larger time steps ($\Delta t = 0.5$) with minimal error ($E_\infty \approx 6.58 \times 10^{-4}$). Von Neumann stability analysis applied to the spatial discretization of the MOL framework confirms neutral stability, with iRK-5 providing a larger stability margin along the imaginary axis compared to RK-4. Grid refinement tests for the inhomogeneous model further confirm that spatial resolution (Δx) dominates total accuracy; reducing Δx from 0.01 to 0.0003 successfully decreases the Mean Square Error from 10^{-3} to 10^{-7}. Overall, both the semi-analytical DTM and numerical MOL(iRK-5) frameworks prove to be highly accurate, robust, and effective standalone tools for investigating complex nonlinear dispersive wave dynamics.

Keywords
KdV-BBM, iRK-5, Cauchy boundary, DTM, MOL

Received: 25 May 2026, Accepted: 6 August 2026
https://doi.org/10.26554/sti.2026.11.4.1497-1515

1. INTRODUCTION

The Korteweg-de Vries-Benjamin-Bona-Mahony (KdV-BBM) equation is a fundamental nonlinear wave model used to describe the propagation of long waves in various physical media, including surface water in channels and shallow seas. By combining the dispersive properties of the BBM equation with the nonlinear characteristics of the classical KdV equation, the KdV-BBM model provides enhanced mathematical stability and physical accuracy for modeling solitary waves that retain their shape and velocity over long distances (Hossain et al., 2025; Khatun and Akbar, 2024; Ramli et al., 2017). This makes it especially well-suited for modeling solitary waves that retain their shape over long distances (Hossain et al., 2025; Khatun and Akbar, 2024; Sarker et al., 2024). However, due to its complex structure involving both non-local dispersion and strong nonlinear advection terms, obtaining exact closed-form analytical solutions remains exceptionally challenging, thereby necessitating sophisticated semi-analytical and high-order numerical strategies (Polwang et al., 2025; Suebcharoen et al., 2022). Current research continues to explore the propagation of regularities and the evolution of the radius of analyticity in fifth-order KdV-BBM models (Carvajal and Panthee, 2022; Mebrate et al., 2024; Tegegn et al., 2023). Lie symmetry analysis has also been applied to obtain conservation laws for higher dimensional extensions (Saha Ray et al., 2020), while other numerical approaches like the Crank-Nicolson scheme mixed finite element have been investigated for fractional variants (Wang et al., 2025). Despite these developments, existing numerical approaches frequently encounter a fundamental trade-off: lower-order implicit schemes like Crank-Nicolson are constrained by limited temporal accuracy ($O(\Delta t^2)$), whereas standard explicit integrators like Fourth-Order Runge-Kutta (RK4) demand excessively small time steps to maintain numerical stability without introducing artificial dissipation or phase errors (Gao et al., 2025; Habibah et al., 2025a).

To establish a rigorous analytical benchmark, the Differential Transform Method (DTM), originally introduced by Zhou (1986), has emerged as a highly efficient semi-analytical approach. DTM constructs solutions in rapidly converging power series form without requiring restrictive perturbation or linearization assumptions (Ayaz, 2004; Habibah et al., 2025a). In this study, DTM is strategically tailored to two distinct physical configurations of the KdV-BBM model: homogeneous and inhomogeneous cases under specific initial conditions. For the homogeneous case, a key methodological refinement lies in the strategic implementation of prescribed Cauchy boundary conditions, which supply essential derivative data to guarantee coefficient uniqueness and accelerate series convergence (Brociek and Pleszczyński, 2024; Hossain et al., 2025). For the second case (inhomogeneous), the application of Nayar's Theorem is integrated into the DTM framework. This theorem is utilized to handle specific variable complexities, thereby facilitating a more efficient derivation of the series solution. While previous literature has explored various extensions of DTM, such as the integration of Nayar's Theorem for handling specific separable variables (Nayar and Phiri, 1974; Odibat, 2008), this research prioritizes the robustness of Cauchy-based DTM for the KdV-BBM framework. The versatility and efficiency of DTM and its reduced variants have been well-established across complex partial differential systems, including convection-reaction-diffusion models (Muhammad et al., 2025), relativistic equations (Faishal and Hasan, 2025), nonlinear dispersive equations models such as the Dullin-Gottwald-Holm equation (Babayar-Razlighi and Soltanalizadeh, 2022), and chemical kinetics systems (Qin and Lou, 2021; Aris Izzuddin Razali and Azliza Abd Latif, 2022).

While semi-analytical methods like DTM provide exact series solutions within their domain of convergence, continuous numerical simulation of long-term wave dynamics over extended spatio-temporal domains requires a high-order numerical scheme (Liu et al., 2024; Pava, 2018). To bridge this gap, the Method of Lines (MOL) offers an elegant spatial-discretization strategy that transforms the governing PDE into a stiff system of Ordinary Differential Equations (ODEs) (Alshareef and Bakodah, 2025; Meyer, 1978; Voigt, 1979). MOL is highly regarded for its physical interpretability and versatility across diverse physical engineering domains, including heat conduction phenomena (Nolasco Serna et al., 2022; Sweilam et al., 2025), solute transport in porous media, spatio-temporal pharmacometrics (Cheng and Li, 2026), and nonlinear dispersive wave models such as the KdV equation (Alshareef and Bakodah, 2025), and the Gardner equation (Putri and Habibah, 2026). The primary rationale for utilizing a newly developed improved fifth-order Runge–Kutta (iRK-5) scheme as the temporal solver within MOL lies in overcoming the stiffness and dispersion errors inherent in traditional solvers. Derived via an optimized Taylor series expansion for stiff initial value problems (Habibah et al., 2025a) based on Verwer and Sanz-Serna's convergence foundations (Verwer and Sanz-Serna, 1984), the iRK-5 scheme delivers superior temporal precision ($O(\Delta t^5)$) and expanded stability domains. When applied to the MOL-discretized KdV-BBM system, iRK-5 effectively mitigates artificial numerical dissipation, prevents amplitude attenuation, and preserves physical phase characteristics even under larger time steps ($\Delta t = 0.5$), thereby surpassing the computational limitations of RK4 and Crank–Nicolson schemes.

The main research gap identified in the existing literature is the lack of a comprehensive comparative study evaluating both optimized series-based semi-analytical techniques and non-dissipative high-order numerical integrators for non-local dispersive PDEs under unified physical scenarios. Addressing this gap constitutes the primary motivation and scientific novelty of this work. This paper offers a dual computational framework, an optimized semi-analytical approach via DTM (enhanced by Cauchy conditions and Nayar's Theorem), and an advanced numerical solver via MOL integrated with the iRK-5 scheme. It is demonstrated that both methodologies independently solve the homogeneous and inhomogeneous KdV-BBM equations with exceptional accuracy. For the homogeneous case, the accuracy and phase-preservation capabilities of MOL(iRK-5) are comprehensively benchmarked against RK4, Crank-Nicolson, and the exact DTM series solutions. Furthermore, the inhomogeneous case is systematically analyzed under various spatial (Δx) and temporal (Δt) discretizations to evaluate grid refinement effects and structural numerical stability.

The overarching novelty of this research lies in the synergistic integration of a high-precision semi-analytical benchmark with an advanced numerical integrator. This work introduces a dual computational approach that couples DTM optimized by Cauchy conditions and Nayar's Theorem with the MOL utilizing the recently developed iRK-5 scheme. The remainder of this paper is organized as follows: Section 3 outlines the theoretical foundations of the Differential Transform Method (DTM). Section 4 details the experimental section, including the benchmark test problems, experimental setup, error metrics, and implementation protocols. Section 5 presents the results and discussion, covering the derivation of exact solutions for homogeneous and inhomogeneous KdV–BBM equations, long-term numerical simulations via MOL-iRK-5, and comprehensive stability analyses. Finally, Section 6 provides the concluding remarks and future research directions.

2. EXPERIMENTAL SECTION

2.1 Benchmark Test Problems and Justification

To rigorously assess the computational performance, accuracy, and physical fidelity of the proposed DTM and MOL(iRK-5) frameworks, two distinct mathematical configurations of the KdV-BBM equation are established as benchmark test problems: a homogeneous solitary wave model and an inhomogeneous forced wave model. The selection of these specific test problems is intentionally designed to present severe computational challenges that test the limits of both semi-analytical and numerical solvers:

1. Case 1: Homogeneous Solitary Wave Propagation

This test problem incorporates strong non-local dispersive terms combined with non-linear advection under Cauchy boundary conditions. Solitary waves represent a uniquely challenging benchmark because numerical algorithms must maintain steep spatial wave gradients, preserve exact soliton peak amplitude, and ensure constant phase velocity over extended temporal horizons (T = 30) without introducing artificial numerical dissipation, amplitude attenuation, or spurious phase lag.

2. Case 2: Inhomogeneous Forced Dispersive Wave System

To evaluate the versatility of the proposed solvers under external driving forces, an inhomogeneous KdV–BBM model incorporating a non-zero spatio-temporal forcing term is examined. This configuration introduces complex non-separable source terms and variable recurrence relations, providing a highly demanding benchmark to verify the applicability of Nayar's Theorem within DTM and testing the structural stability of MOL(iRK-5) under spatial grid refinements (Δx).

While additional initial and boundary configurations could be formulated, the selected homogeneous and inhomogeneous benchmarks comprehensively encompass both localized solitary wave dynamics and non-local forced wave behavior. Consequently, these test problems are sufficiently rigorous and challenging to demonstrate the superiority, phase preservation, and robust convergence of the proposed computational frameworks over conventional RK-4 and Cran-Nicolson schemes.

2.2 Theoretical Foundations of Differential Transformation Method

DTM was introduced and first used by Zhou (1986). He applied this method to solve several PDEs that arise in electrical problems (Zhou, 1986). DTM is based on a truncated Taylor series expansion that transforms differential equations into a system of recurrence relations. For equations involving two independent variables, such as space x and time t, we use the two-dimensional DTM, defined as follows:

Definition 1 If u(x, t) is analytic and continuously differentiable at (0,0), the differential transform of u(x, t) is given by (Khatun and Akbar, 2024):

$$U(k,h) = \frac{1}{k!h!}\left[\frac{\partial^{k+h}u(x,t)}{\partial x^k \partial t^h}\right]_{x=0,t=0}. \quad (1)$$

where k and h are non-negative integers. The inverse differential transform reconstructs the solution as a power series:

Definition 2 The inverse differential transform of U(k, h) is the function u(x, t) itself, and is given by (Khatun and Akbar, 2024).

$$u(x,t) = \sum_{k=0}^{\infty}\sum_{h=0}^{\infty} U(k,h)x^k t^h. \quad (2)$$

Based on Equation (1) and Equation (2), it will be obtained in Equation (3):

$$u(x,t) = \sum_{k=0}^{\infty}\sum_{h=0}^{\infty} \frac{1}{k!h!}\left[\frac{\partial^{k+h}u(x,t)}{\partial x^k \partial t^h}\right]_{x=0,t=0} x^k t^h. \quad (3)$$

which closely resembles the two variable Maclaurin series expansion. Thus, U(k,h) serves as the coefficient of the $x^k t^h$ term in the series in Equation (4):

$$\begin{aligned} u(x,t) = {} & U(0,0)x^0t^0 + U(1,0)x^1t^0 + U(0,1)x^0t^1 \\ & + U(1,1)x^1t^1 + U(2,0)x^2t^0 + U(0,2)x^0t^2 \\ & + U(1,2)x^1t^2 + \cdots \end{aligned} \quad (4)$$

so, it can be said that U(k, h) are the coefficients of the power series terms. Some basic theorems needed to determine differential transformations of sums, multiplications, and partial derivatives of functions in two variables are presented below (Ayaz, 2004; Habibah et al., 2025b; Nayar and Phiri, 1974). All these results follow directly from Definition 1.

Theorem 1 If $w(x,t) = u(x,t) + v(x,t)$, then the differential transform of w is $W(k,h) = U(k,h) + V(k,h)$.

Theorem 2 If $w(x,t) = \lambda u(x,t)$ for any constant $\lambda \in R$, then $W(k,h) = \lambda U(k,h)$.

Theorem 3 If $w(x,t) = ux$, then the transform is $W(k,h) = (k+1)U(k+1,h)$.

Theorem 4 If $w(x,t) = ut$, then $W(k,h) = (h+1)U(k,h+1)$.

Theorem 5 If $w(x,t) = \dfrac{\partial^{r+s}u}{\partial x^r \partial t^s}$, then the corresponding differential transform is $W(k,h) = (k+1)(k+2)\cdots(k+r)(h+1)(h+2)\cdots(h+s)U(k+r,h+s)$.

Theorem 6 If $w(x,t) = u(x,t)v(x,t)$, then the transform of the product is $W(k,h) = \sum_{r=0}^{k}\sum_{s=0}^{h} U(r,h-s)V(k-r,s)$.

Theorem 7 If $w(x,t) = u_x$, then the two-dimensional differential transform of w is given by $W(k,h) = \sum_{r=0}^{k}\sum_{s=0}^{h}(k-r+1)U(r,h-s)U(k-r+1,s)$.

Theorem 8 If $w(x,t) = u_{xxx}$, then its differential transform satisfies $W(k,h) = (k+3)(k+2)(k+1)U(k+3,h)$.

Theorem 9 If $w(x,t) = u_{xxt}$, then $W(k,h) = (h+1)(k+2)(k+1)U(k+2,h+1)$.

Theorem 10 Suppose that the function $u(x,t)$ of two independent variables x and t is separable, i.e., $u(x,t) = f(x)g(t)$, and assume that $u(x,0) = f(x)$. Then, for any pair of non-negative integers (k,h), the differential transform of $u(x,t)$ satisfies $U(k,h) = \frac{1}{f(0)}U(k,0)U(0,h)$, $f(0) \neq 0$, where $U(k,h)$ denotes the two-dimensional differential transform of $u(x,t)$.

2.3 Experimental Setup and Model Configurations

The numerical experiments were systematically structured around two main mathematical models to evaluate solver capabilities under distinct boundary and source conditions. The first configuration considers the homogeneous KdV-BBM equation, formulated as $u_t + u_x - \gamma u_{xxt} + \beta u_{xxx} + \alpha u u_x = 0$. The benchmark physical parameters were selected as $\alpha = 1$, $\beta = 1$, and $\gamma = 1$, with a characteristic wave velocity of v = 1.5. Simulations were carried out over an extended spatial domain [-40,80] using a spatial grid size of $\Delta x = 0.25$ and a temporal step size of $\Delta t = 0.1$ up to T = 30. To establish a comprehensive performance baseline, the proposed Method of Lines coupled with an improved fifth-order Runge-Kutta integrator MOL(iRK-5) was directly benchmarked against both the standard explicit Fourth-Order Runge-Kutta (RK-4) scheme and the implicit Crank-Nicolson (C-N) method.

The second configuration extends the analysis to an inhomogeneous KdV-BBM model defined as a periodic initial-value problem on the compact spatio-temporal domain $((x, t) \in [0, 1] \times [0, 1]$, driven by a prescribed forcing function $g(x, t)$. To thoroughly examine numerical stability and convergence behaviors under grid refinement, extensive parametric sweeps were executed. The spatial refinement study evaluated step sizes across $\Delta x \in \{0.01, 0.002, 0.001, 0.0005, 0.0004, 0.0003\}$, while the temporal sensitivity was assessed using time increments of $\Delta t \in \{10^{-3}, 10^{-4}, 10^{-5}\}$.

2.4 Configurations Error Metrics for Performance Assessment

To quantitatively assess the fidelity, dissipation, and phase preservation of the solvers, four distinct error metrics were calculated at each evaluation step:

1. Maximum Absolute Error (E_∞):

$$E_\infty = \max_{1 \le i \le N} |u_{\text{exact}}(x_i, t) - u_{\text{num}}(x_i, t)|$$

2. Mean Absolute Error (E_R):

$$E_R = \frac{1}{N} \sum_{i=1}^{N} |u_{\text{exact}}(x_i, t) - u_{\text{num}}(x_i, t)|$$

3. Root Mean Square Error (E_K):

$$E_K = \sqrt{\frac{1}{N} \sum_{i=1}^{N} |u_{\text{exact}}(x_i, t) - u_{\text{num}}(x_i, t)|^2}$$

4. Relative Mean Square Error (E_{RMSE}):

$$E_{\text{RMSE}} = \sqrt{\frac{\sum_{i=1}^{N} |u_{\text{exact}}(x_i, t) - u_{\text{num}}(x_i, t)|^2}{\sum_{i=1}^{N} |u_{\text{exact}}(x_i, t)|^2}}$$

2.5 Implementation Protocol

The computational workflow for solving the KdV-BBM equation was executed in three sequential phases to ensure mathematical consistency and numerical accuracy. First, semi-analytical benchmarks were derived using the two-dimensional Differential Transformation Method (2D-DTM), employing Cauchy boundary conditions for the homogeneous model and Nayar's Theorem for the inhomogeneous periodic case. The resulting symbolic series solutions were truncated at higher-order terms to serve as high-precision baseline solutions that approach exact analytical limits. Next, spatial discretization was performed via second-order central finite differences ($O(\Delta x^2)$), effectively transforming the governing partial differential equations (PDEs) into a coupled system of continuous-time ordinary differential equations (ODEs). Boundary conditions were rigorously integrated using boundary derivative elimination for non-periodic boundaries and circulant matrix operators to accommodate periodic domains. Finally, the discrete ODE system was advanced through time using the stage coefficients of the improved fifth-order Runge-Kutta (iRK-5) integrator. Computational efficiency and solver performance were continuously tracked by measuring both accumulated error dynamics and total CPU runtime across all simulation runs.

3. RESULT AND DISCUSSION

This section demonstrates the implementation of DTM to solve both homogeneous and inhomogeneous KdV-BBM equations, where Cauchy boundary conditions are utilized to resolve the homogeneous case and Nayar's Theorem (Theorem 10) is incorporated for the inhomogeneous problem to efficiently derive exact solutions. Beyond evaluating exact solutions, the numerical performance, computational accuracy, and physical fidelity of the proposed dual computational framework comprising the semi-analytical Differential Transform Method (DTM) and the numerical Method of Lines coupled with the improved fifth-order Runge-Kutta scheme (MOL-iRK-5) are comprehensively analyzed. To rigorously benchmark these solvers, two distinct wave propagation regimes of the KdV-BBM equation are examined: a homogeneous solitary wave system and an inhomogeneous forced dispersive wave model. The homogeneous solitary wave problem presents a severe computational test, as the solver must maintain the delicate non-dissipative physical balance between non-linear advective steepening ($\alpha u u_x$) and dispersive spreading ($\beta u_{xxx} and - \gamma u_{xxt}$) without introducing artificial dissipation, amplitude decay, or phase lag over long temporal horizons (T = 30). Conversely, the inhomogeneous case incorporates an external spatio-temporal forcing term $f(x, t)$ physically representing external energy injection such as atmospheric pressure fluctuations or bottom bathymetry variations which generates forced wave trains and non-linear resonance interactions. As detailed in the following subsections, the numerical experiments demonstrate that both proposed schemes not only achieve superior high-order convergence and computational efficiency compared to standard RK-4 and Crank–Nicolson methods, but also perfectly preserve the physical conservation laws, peak wave amplitudes, and phase velocities inherent to the KdV-BBM dynamics.

3.1 Exact Solution for the Homogeneous KdV-BBM Equation Using Differential Transformation Method

This section demonstrates the implementation of DTM to solve both homogeneous and inhomogeneous KdV–BBM equations. We utilize Cauchy boundary conditions to resolve the homogeneous case to efficiently derive exact solutions. Consider the KdV-BBM equation given by Equation (5).

$$u_t + u_x - \gamma u_{xxt} + \beta u_{xxx} + \alpha u u_x = 0 \tag{5}$$

with Cauchy boundary conditions.

$$q_1(t) = u(0,t) = A\,\mathrm{sech}^2(-Bvt) \tag{6}$$

$$q_2(t) = u_x(0,t) = -2AB\,\mathrm{sech}^2(-Bvt)\,\tanh(-Bvt) \tag{7}$$

with A and B:

$$A = \frac{3(v-1)}{\alpha} \qquad \text{and} \qquad B = \frac{1}{2}\sqrt{\frac{v-1}{\gamma v + \beta}}$$

The initial condition associated with KdV-BBM equation (5) given by:

$$p(x) = u(x,0) = A\,\mathrm{sech}^2(Bx) \tag{8}$$

Applying the two-dimensional Differential Transformation Method rules based on Theorems 5, 7, 8, and 9 to each individual differential component yields:

1. Temporal derivative (u_t):

$$D\{u_t\} = (h+1)U(k,h+1)$$

2. Spatial derivative (u_x):

$$D\{u_x\} = (k+1)U(k+1,h)$$

3. Third-order spatial dispersion (βu_{xxx}):

$$D\{\beta u_{xxx}\} = \beta(k+3)(k+2)(k+1)U(k+3,h)$$

4. Nonlinear advection term ($\alpha u u_x$) via 2D discrete convolution:

$$D\{\alpha u u_x\} = \alpha \sum_{r=0}^{k}\sum_{s=0}^{h} U(r,h-s)(k-r+1) \times U(k-r+1,s)$$

5. Mixed spatio-temporal derivative (-γu_{xxt}):

$$D\{-\gamma u_x xt\} = -\gamma(k+2)(k+1)(h+1)U(k+2,h+1)$$

Substituting these individual transformed components back into Equation (5) yields the complete unisolated transformed equation:

$$\begin{aligned}&(h+1)U(k,h+1) + (k+1)U(k+1,h)\\ &\quad + \beta(k+3)(k+2)(k+1)U(k+3,h)\\ &\quad + \alpha\sum_{r=0}^{k}\sum_{s=0}^{h} U(r,h-s)(k-r+1)U(k-r+1,s)\\ &\quad - \gamma(k+2)(k+1)(h+1)U(k+2,h+1) = 0.\end{aligned} \tag{9}$$

Rearranging Equation (9) to group terms containing the temporal derivative coefficient (h+1) on the left-hand side and isolating U(k, $h+1$) provides the explicit, solvable recurrence relation:

$$\begin{aligned}U(k+2,h+1) = \frac{1}{\gamma(k+2)(k+1)(h+1)}\Big[&(h+1)U(k,h+1)\\ &+ (k+1)U(k+1,h)\\ &+ \alpha\sum_{r=0}^{k}\sum_{s=0}^{h} U(r,h-s)(k-r+1)\\ &\quad \times U(k-r+1,s)\\ &+ \beta(k+3)(k+2)(k+1)U(k+3,h)\Big]\end{aligned} \tag{10}$$

The initial condition of the KdV-BBM equation (5) is Equation (8), then the initial value is transformed into $U(k,0)$ using the definition of differential transformation (1), such that we obtain the value of $U(k,0)$ in Equation (11):

$$U(k,0) = \frac{p^{(k)}(0)}{k!}, \qquad k = 0,1,2, \tag{11}$$

For k=0,1,2,3,4,5,6 the value of $U(k,0)$ is given as follows.

$$\begin{aligned}&U(0,0) = A, \quad U(1,0) = 0, \quad U(2,0) = -AB^2,\\ &U(3,0) = 0, \quad U(4,0) = \frac{2}{3}AB^4,\\ &U(5,0) = 0, \quad U(6,0) = -\frac{17}{45}AB^6.\end{aligned}$$

From the first boundary conditions (6) and second boundary (7) we obtain

$$U(0,h) = \frac{q_1^{(h)}}{h!}, \qquad h = 1,2,3,\ldots \tag{12}$$

$$U(1,h) = \frac{q_2^{(h)}}{h!}, \qquad h = 1,2,3,\ldots \tag{13}$$

The next step is to calculate Equation (10) using the value of $U(k,0)$, $U(0,h)$, and $U(1,h)$ to get the values of $U(k,h)$. Using boundary conditions (12) and (13) we obtain $U(0,1)$ and $U(1,1)$ respectively in Equation (14) and (15).

$$U(0,1) = \frac{q_1'(0)}{1!} = 0 \tag{14}$$

$$U(1,1) = \frac{q_2'(0)}{1!} = 2AB^2v \tag{15}$$

For k = 0,1,2,3, the transformation results are given as follows, respectively.

$$\begin{aligned}U(2,1) = \frac{1}{2\gamma}\Big(&U(0,1) + U(1,0)\\ &+ \alpha U(0,0)U(1,0) + 6\beta U(3,0)\Big) = 0.\end{aligned} \tag{16}$$

$$U(3,1)=\frac{1}{6\gamma}\Big[2U(1,1)U(2,0)+\alpha\big(2U(0,0)U(2,0)+U(1,0)^2\big)+24\beta U(4,0)\Big]=-\frac{8}{3}AB^4v. \tag{17}$$

$$U(4,1)=\frac{1}{12\gamma}\Big[2U(2,1)+3U(3,0)+\alpha\big(3U(0,0)U(3,0)+2U(1,0)U(2,0)+U(2,0)U(1,0)\big)+60\beta U(5,0)\Big]=0. \tag{18}$$

$$U(5,1)=\frac{1}{20\gamma}\Big[U(3,1)+4U(4,1)+\alpha\big(4U(0,0)U(4,0)+4U(1,0)U(3,0)+2U(2,0)^2\big)+120\beta U(6,0)\Big]=\frac{34}{15}AB^6v. \tag{19}$$

From boundary conditions (12) and (13) we obtain $U(0,2)$ and $U(1,2)$ respectively.

$$U(0,2)=\frac{q_1''(0)}{2!}=-AB^2v^2 \tag{20}$$

$$U(1,2)=\frac{q_2''(0)}{2!}=0 \tag{21}$$

For $k=0,1,2$, the transformation results are given as follows, respectively.

$$U(2,2)=\frac{1}{4\gamma}\Big[2U(0,2)+U(1,1)+\alpha\big(U(0,1)U(1,0)+U(0,0)U(1,1)\big)+6\beta U(3,1)\Big]=4AB^4v^2. \tag{22}$$

$$U(3,2)=\frac{1}{12\gamma}\Big[2U(1,2)+2U(2,1)+\alpha\big(2U(0,1)U(2,0)+2U(0,0)U(2,1)+U(1,1)U(1,0)+U(1,0)U(1,1)\big)+24\beta U(4,1)\Big]=0. \tag{23}$$

$$U(4,2)=\frac{1}{24\gamma}\Big[2U(2,2)+3U(3,1)+\alpha\big(3U(0,1)U(3,0)+3U(0,0)U(3,1)+2U(1,1)U(2,0)+2U(1,0)U(2,1)+U(2,1)U(1,0)+U(2,0)U(1,1)\big)+60\beta U(5,1)\Big]=-\frac{17}{3}AB^6v^2. \tag{24}$$

From boundary conditions (12) and (13) we obtain $U(0,3)$ and $U(1,3)$ respectively.

$$U(0,3)=\frac{q_1'''(0)}{3!}=0, \tag{25}$$

$$U(1,3)=\frac{q_2'''(0)}{3!}=-\frac{8}{3}AB^4v^3 \tag{26}$$

For k=0,1, the transformation results are given as follows, respectively.

$$U(2,3)=\frac{1}{6\gamma}\Big[3U(0,3)+U(1,2)+\alpha\big(U(0,2)U(1,0)+U(0,1)U(1,1)+U(0,0)U(1,2)\big)+6\beta U(3,2)\Big]=0. \tag{27}$$

$$U(3,3)=\frac{1}{18\gamma}\Big[3U(1,3)+2U(2,2)+\alpha\big(2U(0,2)U(2,0)+2U(0,1)U(2,1)+2U(0,0)U(2,2)+U(1,2)U(1,0)+U(1,1)^2+U(1,0)U(1,2)\big)+24\beta U(4,2)\Big]=\frac{68}{9}AB^6v^3. \tag{28}$$

Substitute Equation (14) to Equation (28) into Equation (2) then we get

$$\begin{aligned}
u(x,t) &= \sum_{k=0}^{\infty}\sum_{h=0}^{\infty} U(k,h)x^k t^h \\
&= U(0,0) + U(0,1)t + U(0,2)t^2 + U(0,3)t^3 \\
&\quad + U(0,4)t^4 + U(0,5)t^5 + U(0,6)t^6 \\
&\quad + U(1,0)x + U(1,1)xt + U(1,2)xt^2 + U(1,3)xt^3 \\
&\quad + U(1,4)xt^4 + U(1,5)xt^5 \\
&\quad + U(2,0)x^2 + U(2,1)x^2t + U(2,2)x^2t^2 \\
&\quad + U(2,3)x^2t^3 + U(2,4)x^2t^4 \\
&\quad + U(3,0)x^3 + U(3,1)x^3t + U(3,2)x^3t^2 \\
&\quad + U(3,3)x^3t^3 + \cdots \\
&= A - AB^2x^2 + \frac{2}{3}AB^4x^4 - \frac{17}{45}AB^6x^6 \\
&\quad + 2AB^2vxt - \frac{8}{3}AB^4vx^3t + \frac{34}{15}AB^6vx^5t \\
&\quad - AB^2v^2t^2 + 4AB^4v^2x^2t^2 - \frac{17}{3}AB^6v^2x^4t^2 \\
&\quad - \frac{8}{3}AB^4v^3xt^3 + \frac{68}{9}AB^6v^3x^3t^3 + \cdots \\
&= A\,\mathrm{sech}^2(B(x-vt)).
\end{aligned} \tag{29}$$

By identifying the patterns in the determined coefficients $U(k,h)$ and comparing them with the Maclaurin expansion of hyperbolic functions, the resulting power series can be expressed in the following closed-form exact solution KdV-BBM in Equation (29). This con- firms that the proposed DTM framework, enhanced by Cauchy conditions, successfully recovers the exact analytical solution for the solitary wave.

3.2 Exact Solution for the Inhomogeneous KdV-BBM Equation Using Differential Transformation Method

Consider the following periodic initial value problem of the inhomogeneous BBM–KdV equation:

$$u_t - u_{xxt} + u_{xxx} + u_x + uu_x = g(x,t), \qquad (x,t) \in [0,1]\times[0,1]. \tag{30}$$

where

$$\begin{aligned}
g(x,t) = e^{-t}\Big[&-\sin(2\pi x)(1+4\pi^2) \\
&+ \cos(2\pi x)(-8\pi^3 + 2\pi) \\
&+ \pi\sin(4\pi x)e^{-t}\Big],
\end{aligned}$$

and the initial condition is

$$u(x,0) = \sin(2\pi x). \tag{31}$$

The initial stage of the method is to determine the differential transform of initial condition (31). From the Taylor series expansion of this function, its differential transform is obtained as:

$$U(k,0) = \frac{(2\pi)^k}{k!}\sin\left(\frac{k\pi}{2}\right). \tag{32}$$

The result of the transformation for Equation (30) is obtained as follows.

$$\begin{aligned}
&(h+1)U(k,h+1) - (h+1)(k+2)(k+1)U(k+2,h+1) \\
&\quad + (k+3)(k+2)(k+1)U(k+3,h) + (k+1)U(k+1,h) \\
&\quad + \sum_{r=0}^{k}\sum_{s=0}^{h} U(r,h-s)(k-r+1)U(k-r+1,s) \\
&\quad = G(k,h),
\end{aligned} \tag{33}$$

where

$$\begin{aligned}
G(k,h) = \frac{1}{k!h!}\Big\{(-1)^h(2\pi)^k\Big[&-(1+4\pi^2)\sin\left(\frac{k\pi}{2}\right) \\
&+ (-8\pi^3+2\pi)\cos\left(\frac{k\pi}{2}\right)\Big] \\
&+ (-2)^h\pi(4\pi)^k\sin\left(\frac{k\pi}{2}\right)\Big\}.
\end{aligned}$$

Equation (33) can be rewritten as follows.

$$\begin{aligned}
&(h+1)U(k,h+1) - (h+1)(k+2)(k+1)U(k+2,h+1) \\
&= -(k+3)(k+2)(k+1)U(k+3,h) - (k+1)U(k+1,h) \\
&\quad - \sum_{r=0}^{k}\sum_{s=0}^{h} U(r,h-s)(k-r+1)U(k-r+1,s) \\
&\quad + G(k,h).
\end{aligned} \tag{34}$$

For h=0, the transformation results in (34) is given as follows.

$$\begin{aligned}
U(k,1) &- (k+2)(k+1)U(k+2,1) \\
&= -(k+3)(k+2)(k+1)U(k+3,0) \\
&\quad - (k+1)U(k+1,0) \\
&\quad - \sum_{r=0}^{k} U(r,0)(k-r+1)U(k-r+1,0) \\
&\quad + G(k,0).
\end{aligned} \tag{35}$$

Substituting the initial condition (32) and simplifications reduce Equation (35) to the following form:

$$
\begin{aligned}
&U(k,1)-(k+2)(k+1)U(k+2,1)\\
&\quad= -\frac{(2\pi)^{k+3}}{k!}\sin\left(\frac{(k+3)\pi}{2}\right)\\
&\qquad-\frac{(2\pi)^{k+1}}{k!}\sin\left(\frac{(k+1)\pi}{2}\right)\\
&\qquad-\sum_{r=0}^{k}\frac{(2\pi)^{k+1}}{r!(k-r)!}\sin\left(\frac{r\pi}{2}\right)\\
&\qquad\quad\times\sin\left(\frac{(k-r+1)\pi}{2}\right)\\
&\qquad+\frac{1}{k!}\Bigg[(2\pi)^{k}\Bigg(-(1+4\pi^2)\sin\left(\frac{k\pi}{2}\right)\\
&\qquad\qquad+(-8\pi^3+2\pi)\cos\left(\frac{k\pi}{2}\right)\Bigg)\\
&\qquad\qquad+\pi(4\pi)^k\sin\left(\frac{k\pi}{2}\right)\Bigg]\\
&\quad=\frac{(2\pi)^k}{k!}\Bigg[-(2\pi)^3\sin\left(\frac{(k+3)\pi}{2}\right)\\
&\qquad-2\pi\sin\left(\frac{(k+1)\pi}{2}\right)\\
&\qquad-2\pi\sum_{r=0}^{k}\binom{k}{r}\sin\left(\frac{r\pi}{2}\right)\\
&\qquad\quad\times\sin\left(\frac{(k-r+1)\pi}{2}\right)\\
&\qquad-(1+4\pi^2)\sin\left(\frac{k\pi}{2}\right)\\
&\qquad+(-8\pi^3+2\pi)\cos\left(\frac{k\pi}{2}\right)\\
&\qquad+2^k\pi\sin\left(\frac{k\pi}{2}\right)\Bigg].\\
&\quad=\frac{(2\pi)^k}{k!}\Bigg[(8\pi^3-2\pi)\cos\left(\frac{k\pi}{2}\right)\\
&\qquad-(1+4\pi^2)\sin\left(\frac{k\pi}{2}\right)\\
&\qquad-\pi\sum_{r=0}^{k}\binom{k}{r}\cos\left(\frac{(2r-k-1)\pi}{2}\right)\\
&\qquad+\pi 2^k\cos\left(\frac{(k+1)\pi}{2}\right)\\
&\qquad+2^k\pi\sin\left(\frac{k\pi}{2}\right)\Bigg]\\
&\quad=\frac{(2\pi)^k}{k!}\Bigg[-(1+4\pi^2)\sin\left(\frac{k\pi}{2}\right)\\
&\qquad-\pi\sum_{r=0}^{k}\binom{k}{r}\sin\left(\left(r-\frac{k}{2}\right)\pi\right)\\
&\qquad+\pi 2^k\cos\left(\frac{(k+1)\pi}{2}\right)\\
&\qquad+2^k\pi\sin\left(\frac{k\pi}{2}\right)\Bigg].\\
&\quad=\frac{(2\pi)^k}{k!}\Bigg[-(1+4\pi^2)\sin\left(\frac{k\pi}{2}\right)\\
&\qquad+\pi 2^k\cos\left(\frac{(k+1)\pi}{2}\right)+2^k\pi\sin\left(\frac{k\pi}{2}\right)\Bigg]\\
&\quad=\frac{(2\pi)^k}{k!}\left[-(1+4\pi^2)\sin\left(\frac{k\pi}{2}\right)\right].
\end{aligned}
\tag{36}
$$

The left-hand side of the Equation (36) can be simplified by applying Theorem 10 as follows in Equation (37). The simplification of the left-hand side in Equation (36) is strategically achieved by invoking Theorem 10. This approach is justified as the structure of the source term $g(x,t)$ and the periodic initial conditions satisfy the separability assumption $u(x,t)=f(x)g(t)$, thereby allowing the complex recurrence relations to be bypassed efficiently.

$$
\begin{aligned}
&U(k,1)-(k+2)(k+1)U(k+2,1)\\
&\quad=U(k,0)U(0,1)-(k+2)(k+1)U(k+2,0)U(0,1)\\
&\quad=U(0,1)\left[U(k,0)-(k+2)(k+1)U(k+2,0)\right]\\
&\quad=U(0,1)\Bigg[\frac{(2\pi)^k}{k!}\sin\left(\frac{k\pi}{2}\right)\\
&\qquad\quad-(k+2)(k+1)\frac{(2\pi)^{k+2}}{(k+2)!}\sin\left(\frac{(k+2)\pi}{2}\right)\Bigg]\\
&\quad=U(0,1)\frac{(2\pi)^k}{k!}\left[\sin\left(\frac{k\pi}{2}\right)-4\pi^2\sin\left(\frac{k\pi}{2}+\pi\right)\right]\\
&\quad=U(0,1)\frac{(2\pi)^k}{k!}\left[\sin\left(\frac{k\pi}{2}\right)-4\pi^2\left(-\sin\left(\frac{k\pi}{2}\right)\right)\right]\\
&\quad=U(0,1)\frac{(2\pi)^k}{k!}(1+4\pi^2)\sin\left(\frac{k\pi}{2}\right).
\end{aligned}
\tag{37}
$$

Based on the simplification of the right-hand side in (36) and the left-hand side in (37), the following relation is obtained.

$$
\begin{aligned}
&U(0,1)\frac{(2\pi)^k}{k!}(1+4\pi^2)\sin\left(\frac{k\pi}{2}\right)\\
&\qquad=\frac{(2\pi)^k}{k!}\left[-(1+4\pi^2)\sin\left(\frac{k\pi}{2}\right)\right],\\
&U(0,1)=-1.
\end{aligned}
$$

Thus, $U(k,1)$ can be evaluated by

$$\begin{aligned}U(k,1) &= U(k,0)U(0,1)\\ &= U(k,0)(-1)\\ &= -\frac{(2\pi)^k}{k!}\sin\left(\frac{k\pi}{2}\right).\end{aligned}$$

To evaluate $U(k,2)$, set $h=1$ so that the transformation results in (34) is given as follows.

$$\begin{aligned}
&2U(k,2) - 2(k+2)(k+1)U(k+2,2)\\
&\quad = -(k+3)(k+2)(k+1)U(k+3,1)\\
&\qquad -(k+1)U(k+1,1)\\
&\qquad -\sum_{r=0}^{k}\sum_{s=0}^{1}U(r,1-s)(k-r+1)\\
&\qquad\quad \times U(k-r+1,s)\\
&\qquad +\frac{(2\pi)^k}{k!}\left[(1+4\pi^2-2^{k+1}\pi)\sin\left(\frac{k\pi}{2}\right)\right.\\
&\qquad\quad \left.+(8\pi^3-2\pi)\cos\left(\frac{k\pi}{2}\right)\right]\\
&\quad = \frac{(2\pi)^{k+3}}{k!}\sin\left(\frac{(k+3)\pi}{2}\right)\\
&\qquad +\frac{(2\pi)^{k+1}}{k!}\sin\left(\frac{(k+1)\pi}{2}\right)\\
&\qquad +\frac{2(2\pi)^{k+1}}{k!}\sum_{r=0}^{k}\binom{k}{r}\sin\left(\frac{r\pi}{2}\right)\\
&\qquad\quad \times\sin\left(\frac{(k-r+1)\pi}{2}\right)\\
&\qquad +\frac{(2\pi)^k}{k!}\left[(1+4\pi^2-2^{k+1}\pi)\sin\left(\frac{k\pi}{2}\right)\right.\\
&\qquad\quad \left.+(8\pi^3-2\pi)\cos\left(\frac{k\pi}{2}\right)\right]\\
&\quad = \frac{(2\pi)^{k+3}}{k!}\sin\left(\frac{(k+3)\pi}{2}\right)\\
&\qquad +\frac{(2\pi)^{k+1}}{k!}\sin\left(\frac{(k+1)\pi}{2}\right)\\
&\qquad -\frac{(2\pi)^{k+1}}{k!}2^k\cos\left(\frac{(k+1)\pi}{2}\right)\\
&\qquad +\frac{(2\pi)^k}{k!}\left[(1+4\pi^2-2^{k+1}\pi)\sin\left(\frac{k\pi}{2}\right)\right.\\
&\qquad\quad \left.+(8\pi^3-2\pi)\cos\left(\frac{k\pi}{2}\right)\right]\\
&\quad = \frac{(2\pi)^{k+1}}{k!}\left[(1-4\pi^2)\sin\left(\frac{(k+1)\pi}{2}\right)\right.\\
&\qquad\quad \left.-2^k\cos\left(\frac{(k+1)\pi}{2}\right)\right]\\
&\qquad +\frac{(2\pi)^k}{k!}\left[(1+4\pi^2-2^{k+1}\pi)\sin\left(\frac{k\pi}{2}\right)\right.\\
&\qquad\quad \left.+(8\pi^3-2\pi)\cos\left(\frac{k\pi}{2}\right)\right]\\
&\quad = \frac{(2\pi)^k}{k!}\left[2\pi\left((1-4\pi^2)\sin\left(\frac{(k+1)\pi}{2}\right)\right.\right.\\
&\qquad\quad \left.-2^k\cos\left(\frac{(k+1)\pi}{2}\right)\right)\\
&\qquad\quad +(1+4\pi^2-2^{k+1}\pi)\sin\left(\frac{k\pi}{2}\right)\\
&\qquad\quad \left.+(8\pi^3-2\pi)\cos\left(\frac{k\pi}{2}\right)\right]\\
&\quad = \frac{(2\pi)^k}{k!}\left[2\pi\left((1-4\pi^2)\cos\left(\frac{k\pi}{2}\right)\right.\right.\\
&\qquad\quad \left.+2^k\sin\left(\frac{k\pi}{2}\right)\right)\\
&\qquad\quad +(1+4\pi^2-2^{k+1}\pi)\sin\left(\frac{k\pi}{2}\right)\\
&\qquad\quad \left.+(8\pi^3-2\pi)\cos\left(\frac{k\pi}{2}\right)\right]\\
&\quad = \frac{(2\pi)^k}{k!}(1+4\pi^2)\sin\left(\frac{k\pi}{2}\right).
\end{aligned} \tag{38}$$

The left-hand side of Equation (38) can be evaluated using the same approach as in Equation (37).

$$
\begin{aligned}
2U(k,2) - 2(k+2)(k+1)U(k+2,2) &= 2\Big(U(k,2) \\
&\quad - (k+2)(k+1)U(k+2,2)\Big) \\
&= 2\Big(U(k,0)U(0,2) \\
&\quad - (k+2)(k+1)U(k+2,0)U(0,2)\Big) \\
&= 2U(0,2)\Big(U(k,0) \\
&\quad - (k+2)(k+1)U(k+2,0)\Big) \\
&= 2U(2,0)\,\frac{(2\pi)^k}{k!} \\
&\quad \times (1+4\pi^2)\sin\left(\frac{k\pi}{2}\right).
\end{aligned} \tag{39}
$$

Based on the right-hand side of (38) and the left-hand side of (39), the following relation is obtained.

$$
2U(2,0)\,\frac{(2\pi)^k}{k!}(1+4\pi^2)\sin\left(\frac{k\pi}{2}\right) = \frac{(2\pi)^k}{k!}(1+4\pi^2)\sin\left(\frac{k\pi}{2}\right)
$$

$$
U(2,0) = \frac{1}{2}.
$$

Thus, the value of $U(k,2)$ can be computed by

$$
\begin{aligned}
U(k,2) &= U(k,0)U(0,2) \\
&= \frac{1}{2}U(k,0) \\
&= \frac{1}{2}\frac{(2\pi)^k}{k!}\sin\left(\frac{k\pi}{2}\right).
\end{aligned}
$$

$U(k,3)$ can also be computed in the same way, yielding

$$
U(k,3) = \frac{(-1)^3}{3!k!}(2\pi)^k\sin\left(\frac{k\pi}{2}\right).
$$

Since $U(k,i)$, for i=0,1,2,3, exhibits the same pattern, the general form of $U(k,h)$ is given

$$
U(k,h) = \frac{(-1)^h}{h!\,k!}(2\pi)^k\sin\left(\frac{k\pi}{2}\right). \tag{40}
$$

Substituting the obtained expression for $U(k,h)$ in (4θ) into the inverse differential transform (2), the solution of the KdV-BBM equation (30) is obtained as:

$$
\begin{aligned}
u(x,t) &= \sum_{k=0}^{\infty}\sum_{h=0}^{\infty}U(k,h)x^k t^h \\
&= \sum_{k=0}^{\infty}\sum_{h=0}^{\infty}\frac{(-1)^h}{h!\,k!}(2\pi)^k\sin\left(\frac{k\pi}{2}\right)x^k t^h \\
&= \left(\sum_{h=0}^{\infty}\frac{(-1)^h}{h!}t^h\right)\left(\sum_{k=0}^{\infty}\frac{(2\pi)^k}{k!}\sin\left(\frac{k\pi}{2}\right)x^k\right) \\
&= e^{-t}\sin(2\pi x).
\end{aligned} \tag{41}
$$

Recognizing the term $\sum_{h=0}^{\infty}\frac{(-t)^h}{h!}$ as the Maclaurin series for e^{-t} and $\sum_{k=0}^{\infty}\frac{(2\pi x)^k}{k!}\sin\left(\frac{k\pi}{2}\right)$ as the Taylor expansion of $\sin(2\pi x)$, we obtain the exact solution of the KdV-BBM equation (30) in Equation (41).

3.3 Numerical Simulation of the Homogeneous KdV-BBM Equation Using Method of Lines Scheme

Consider the KdV–BBM equation (5) subject to the given initial (8) and boundary conditions (6) and (7). Approximate u_x, u_{xx}, and u_{xxx} using second order central finite difference to obtain the following.

$$
\begin{aligned}
\frac{du_i}{dt} &= -\frac{u_{i+1}-u_{i-1}}{2\Delta x} \\
&\quad + \gamma\frac{d}{dt}\left(\frac{u_{i+1}-2u_i+u_{i-1}}{\Delta x^2}\right) \\
&\quad - \beta\frac{u_{i+2}-2u_{i+1}+2u_{i-1}-u_{i-2}}{2\Delta x^3} \\
&\quad - \alpha u_i\left(\frac{u_{i+1}-u_{i-1}}{2\Delta x}\right).
\end{aligned} \tag{42}
$$

Equation (42) can be rearranged into

$$
\begin{aligned}
-\gamma\frac{du_{i-1}}{dt} &+ (\Delta x^2+2\gamma)\frac{du_i}{dt} \\
&- \gamma\frac{du_{i+1}}{dt} \\
&= -\frac{\Delta x}{2}(u_{i+1}-u_{i-1}) \\
&\quad - \frac{\beta}{2\Delta x}\Big(u_{i+2}-2u_{i+1} \\
&\qquad + 2u_{i-1}-u_{i-2}\Big) \\
&\quad - \frac{\alpha\Delta x}{2}u_i(u_{i+1}-u_{i-1}) \\
&= f_i.
\end{aligned} \tag{43}
$$

Equation (43) is to be resolved for $i = 2, 3, \ldots, N-1$. For $i = 1$ and $i = N$, the values are known from the boundary conditions.

For the first interior grid point ($j = 1$), the central difference approximation introduces a fictitious point u_0 which lies outside the physical boundary. This point is systematically eliminated by utilizing the prescribed boundary condition. By applying a central difference to the Neumann boundary condition $\frac{\partial u}{\partial x}(x_1,t) = 0$, we establish the relation $\frac{u_2-u_0}{2\Delta x} = 0$, which yields $u_0 = u_2$. Furthermore, since the value at the boundary u_1 is constant, its temporal derivative $\frac{du_1}{dt}$ vanishes and does not contribute to the dynamic system.

A similar procedure is applied to the last interior point ($j = M-1$), where the fictitious point u_{M+1} is encountered. By

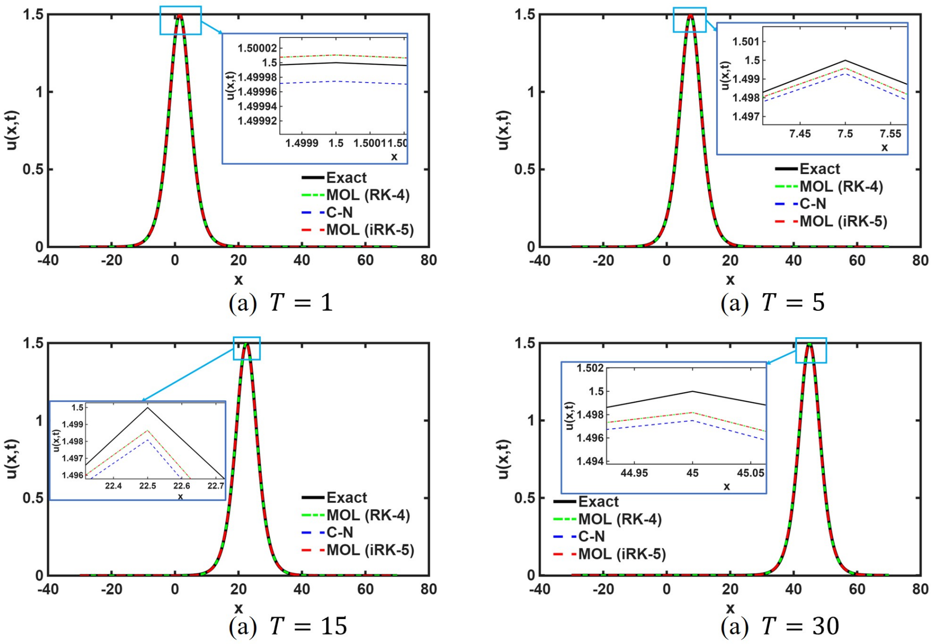

Figure 1. Exact Solution and Numerical Solution of the KdV-BBM Equation With Parameters $\alpha = \beta = \gamma = 1$, $\Delta x = 0.25$, and $\Delta t = 0.1$

invoking the boundary condition at the far end, $\frac{\partial u}{\partial x}(x_M, t) = 0$, we obtain the relation $u_{M+1} = u_{M-1}$. With the boundary value u_M being constant, the time derivative $\frac{du_M}{dt}$ is also zero. These substitutions allow the semi-discrete system to be closed and expressed as a standard system of ODEs, which is then solved using the iRK-5 integrator.

By substituting these relations into the discretized system, the fictitious points and boundary derivatives are eliminated, allowing the system of ordinary differential equations (ODEs) to be expressed in the following matrix form:

$$A \begin{bmatrix} \frac{du_2}{dt} \\ \frac{du_3}{dt} \\ \vdots \\ \frac{du_{N-2}}{dt} \\ \frac{du_{N-1}}{dt} \end{bmatrix} = \begin{bmatrix} -\frac{\Delta x}{2}(u_3-u_1)-\frac{\beta}{2\Delta x}(u_4-2u_3+2u_1-u_2) \\ -\frac{\alpha\Delta x}{2}u_2(u_3-u_1) \\ -\frac{\Delta x}{2}(u_4-u_2)-\frac{\beta}{2\Delta x}(u_5-2u_4+2u_2-u_1) \\ -\frac{\alpha\Delta x}{2}u_3(u_4-u_2) \\ \vdots \\ -\frac{\Delta x}{2}(u_{N-1}-u_{N-3})-\frac{\beta}{2\Delta x}(u_N-2u_{N-1}+2u_{N-3}-u_{N-4}) \\ -\frac{\alpha\Delta x}{2}u_{N-2}(u_{N-1}-u_{N-3}) \\ -\frac{\Delta x}{2}(u_N-u_{N-2})-\frac{\beta}{2\Delta x}(u_{N-1}-2u_N+2u_{N-2}-u_{N-3}) \\ -\frac{\alpha\Delta x}{2}u_{N-1}(u_N-u_{N-2}) \end{bmatrix}. \tag{44}$$

Equation (44) forms a system of ordinary differential equations as follows.

$$\frac{du_i(t)}{dt} = A^{-1} f_i(\vec{u}^{(t)}, t), \qquad i = 2, 3, \ldots, N-1. \tag{45}$$

where $\vec{u}^{(t)} = \left(u_2^{(t)}, u_3^{(t)}, \ldots, u_{N-1}^{(t)}\right)$. The second step of the MOL method is to solve the ODE system (45) using the improved fifth-order Runge-Kutta method [7].

The comparative performance of the iRK-5, RK-4, and Crank-Nicolson methods is quantitatively detailed in Table ?? and visually validated through the soliton profiles in Figure 1a to Figure 1d. For a fixed position at $x = 1.4$, the numerical data in Table ?? reveals that the iRK-5 method consistently yields the highest precision, achieving a minimum error of 7.60×10^{-4} at $t = 1.0$. While the RK-4 method remains highly competitive, the iRK-5 scheme demonstrates a superior ability to approximate the exact solution with finer decimal accuracy. This numerical superiority is further substantiated by the wave profiles in Figure 1, where the magnified insets at the peak of the soliton illustrate that the iRK-5 trajectory aligns most closely with the exact solution across all time intervals from $T = 1$ to $T = 30$. Conversely, the Crank-Nicolson method exhibits noticeable amplitude dissipation and larger deviations, as evidenced by both the higher error values in Table ?? and the visible drop in peak height in the insets of Figure 1d. Ultimately, the synergy between the tabular data and the graphical plots confirms that the iRK-5 method is the most robust and

Table 1. Comparison of Numerical and Exact Solutions at a Fixed Position $x = 1.4$ For the KdV-BBM Equation (5) With Parameters $\Delta x = 0.25$, $\Delta t = 0.1$, $\alpha = \beta = \gamma = 1$, and $v = 1.5$

t	Exact	iRK-5	RK-4	C-N	Error iRK-5	Error RK-4	Error C-N
0.1	1.38865640	1.37116519	1.37116517	1.37114765	1.75×10^{-2}	1.75×10^{-2}	1.75×10^{-2}
0.2	1.41278860	1.39690443	1.39690440	1.39687127	1.59×10^{-2}	1.59×10^{-2}	1.59×10^{-2}
0.3	1.43429789	1.42015802	1.42015797	1.42011170	1.41×10^{-2}	1.41×10^{-2}	1.42×10^{-2}
0.4	1.45300574	1.44073661	1.44073654	1.44068007	1.23×10^{-2}	1.23×10^{-2}	1.23×10^{-2}
0.5	1.46875348	1.45846860	1.45846850	1.45840522	1.03×10^{-2}	1.03×10^{-2}	1.03×10^{-2}
0.6	1.48140515	1.47320306	1.47320295	1.47313663	8.20×10^{-3}	8.20×10^{-3}	8.27×10^{-3}
0.7	1.49084989	1.48481246	1.48481232	1.48474705	6.04×10^{-3}	6.04×10^{-3}	6.10×10^{-3}
0.8	1.49700400	1.49319489	1.49319473	1.49313481	3.81×10^{-3}	3.81×10^{-3}	3.87×10^{-3}
0.9	1.49981252	1.49827607	1.49827588	1.49822574	1.54×10^{-3}	1.54×10^{-3}	1.59×10^{-3}
1.0	1.49925025	1.50001062	1.50001042	1.49997450	7.60×10^{-4}	7.60×10^{-4}	7.24×10^{-4}

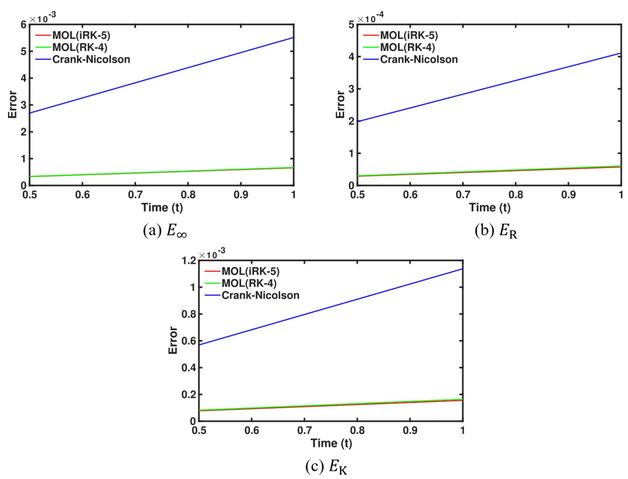

Figure 2. Comparison of (A) E_∞, (B) E_R, and (C) E_K for the MOL(iRK-5), MOL(RK-4), and Crank–Nicolson Methods Applied to the KdV-BBM Equation (5) With $\Delta t = 0.5$ and $\Delta x = 0.25$

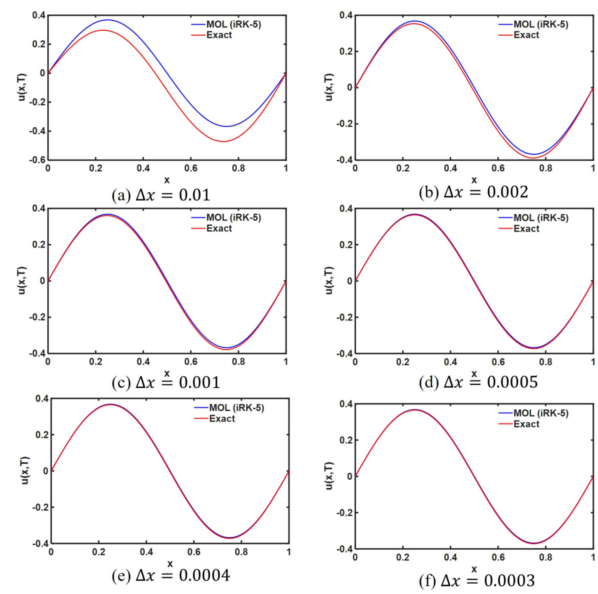

Figure 3. Exact and Numerical Solutions of the KdV-BBM Equation (30) for $\beta = 1$, $\alpha = 1$, $\gamma = 1$, $\Delta t = 0.001$, and Various Values of Δx

efficient scheme for maintaining the physical integrity of nonlinear dispersive waves over extended simulation periods.

The spatial data in Table 2 provides a localized explanation for the wave profile deviations observed in Figure 1. At t = 1.0, the errors for all methods are most pronounced near the peak of the soliton (around x = 1.0 to 2.0), where values reach the magnitude of 10^{-4}. These localized errors correspond directly to the magnified insets in Figure1, where the C-N profile shows a visible drop in peak height and a shift away from the exact solution. In contrast, the iRK-5 method maintains the lowest errors even at the soliton's tail (e.g., $3.77{\times}10^{-6}$ at x = 70.0), ensuring that the physical integrity and amplitude of the dispersive wave are preserved throughout the simulation up to T = 30. Ultimately, the synergy between the tabular data and the graphical evidence confirms that the iRK-5 scheme is the most robust tool for minimizing numerical dissipation in nonlinear wave equations.

According to Table 3, the iRK5 method maintains a superior precision of $6.5847{\times}10^{-4}$ even at a large step of Δt = 0.5. This high level of accuracy is visually confirmed by Figure 2a, where the iRK-5 and RK-4 remain significantly lower and flatter than the Crank-Nicolson method. The steep upward slope of the blue curve in Figure 2a illustrates the rapid accumulation of temporal errors compared to the more stable Runge-Kutta schemes.

A critical observation can be made from Table 4, which displays the Mean Absolute Error (MAE). The data shows that

Table 2. Numerical Results With Parameters $\Delta x = 1$, $\Delta t = 0.1$, $\alpha = \beta = \gamma = 1$, and $\nu = 1.5$

x	Exact	iRK-5	RK-4	C-N	Error iRK-5	Error RK-4	Error C-N
−30.0	4.57×10^{-6}	-3.16×10^{-6}	-3.19×10^{-6}	-3.89×10^{-6}	7.74×10^{-6}	7.76×10^{-6}	8.46×10^{-6}
−29.0	7.15×10^{-6}	3.48×10^{-6}	3.47×10^{-6}	3.18×10^{-6}	3.67×10^{-6}	3.68×10^{-6}	3.97×10^{-6}
−28.0	11.18×10^{-6}	7.84×10^{-6}	7.84×10^{-6}	7.72×10^{-6}	3.34×10^{-6}	3.34×10^{-6}	3.47×10^{-6}
−27.0	17.49×10^{-6}	1.53×10^{-5}	1.53×10^{-5}	1.52×10^{-5}	2.24×10^{-6}	2.24×10^{-6}	2.29×10^{-6}
−26.0	27.35×10^{-6}	2.60×10^{-5}	2.60×10^{-5}	2.59×10^{-5}	1.35×10^{-6}	1.35×10^{-6}	1.38×10^{-6}
⋮	⋮	⋮	⋮	⋮	⋮	⋮	⋮
−3.0	6.24×10^{-1}	6.24×10^{-1}	6.25×10^{-1}	6.25×10^{-1}	4.58×10^{-4}	4.59×10^{-4}	5.02×10^{-4}
−2.0	8.5×10^{-1}	8.58×10^{-1}	8.59×10^{-1}	8.59×10^{-1}	5.92×10^{-4}	5.92×10^{-4}	7.23×10^{-4}
−1.0	1.11404963	1.11463979	1.11463995	1.11483764	5.90×10^{-4}	5.90×10^{-4}	7.88×10^{-4}
0.0	1.34314421	1.34359063	1.34359061	1.34376274	4.46×10^{-4}	4.46×10^{-4}	6.19×10^{-4}
1.0	1.48140515	1.48158573	1.48158555	1.48162831	1.81×10^{-4}	1.80×10^{-4}	2.23×10^{-4}
2.0	1.48140515	1.48123449	1.48123431	1.48113008	1.71×10^{-4}	1.71×10^{-4}	2.75×10^{-4}
3.0	1.34314421	1.34265371	1.34265367	1.34248198	4.90×10^{-4}	4.91×10^{-4}	6.62×10^{-4}
⋮	⋮	⋮	⋮	⋮	⋮	⋮	⋮
66.0	0.00000000	6.30×10^{-7}	6.30×10^{-7}	6.40×10^{-7}	6.28×10^{-7}	6.28×10^{-7}	6.37×10^{-7}
67.0	0.00000000	1.65×10^{-6}	1.65×10^{-6}	1.67×10^{-6}	1.65×10^{-6}	1.65×10^{-6}	1.67×10^{-6}
68.0	0.00000000	2.96×10^{-6}	2.96×10^{-6}	2.96×10^{-6}	2.96×10^{-6}	2.96×10^{-6}	2.96×10^{-6}
69.0	0.00000000	2.19×10^{-6}	2.19×10^{-6}	2.16×10^{-6}	2.19×10^{-6}	2.19×10^{-6}	2.16×10^{-6}
70.0	0.00000000	3.77×10^{-6}	3.76×10^{-6}	3.83×10^{-6}	3.77×10^{-6}	3.76×10^{-6}	3.83×10^{-6}

Table 3. Comparison of Maximum Error (E_∞) for $\Delta x = 0.25$, $\alpha = \beta = \gamma = 1$, and $\nu = 1.5$

Δt	iRK-5	RK-4	C-N
0.5	6.5847×10^{-4}	6.7230×10^{-4}	5.5156×10^{-3}
0.2	6.3333×10^{-4}	6.3301×10^{-4}	1.3793×10^{-3}
0.1	6.3216×10^{-4}	6.3206×10^{-4}	7.9199×10^{-4}
0.05	6.3202×10^{-4}	6.3200×10^{-4}	6.8585×10^{-4}
0.01	6.3200×10^{-4}	6.3200×10^{-4}	6.3338×10^{-4}

Table 4. Comparison of Mean Absolute Error (E_R) for $\Delta x = 0.25$, $\alpha = \beta = \gamma = 1$, and v=1.5

Δt	iRK5	RK4	C-N
0.5	5.7595×10^(-5)	6.0383×10^(-5)	4.1123×10^(-4)
0.2	5.7420×10^(-5)	5.7494 ×10^(-5)	1.0875×10^(-4)
0.1	5.7416×10^(-5)	5.7420×10^(-5)	6.9807×10^(-5)
0.05	5.7415×10^(-5)	5.7415×10^(-5)	6.0444×10^(-5)
0.01	5.7415×10^(-5)	5.7415×10^(-5)	5.7536×10^(-5)

the iRK-5 method reaches a precision level of 5.7420×10^{-5} at a relatively large step of $\Delta t = 0.2$. In contrast, the RK-4 method requires a smaller time step to achieve an equivalent error magnitude. This finding is reinforced by 2b, where the iRK-5 trajectory consistently occupies the lowest position, indicating its superior efficiency in minimizing residual growth over time.

Furthermore, the trends in Figure 2c align perfectly with

Table 5. Comparison of Root Mean Square Error (E_K) for $\Delta x = 0.25$, $\alpha = \beta = \gamma = 1$, And $v = 1.5$

Δt	iRK5	RK4	C-N
0.5	1.5562×10^(-4)	1.6423×10^(-4)	1.1375×10^(-3)
0.2	1.5521×10^(-4)	1.5545×10^(-4)	3.0693×10^(-4)
0.1	1.5521×10^(-4)	1.5522×10^(-4)	1.9165×10^(-4)
0.05	1.5521×10^(-4)	1.5521×10^(-4)	1.6414×10^(-4)
0.01	1.5521×10^(-4)	1.5521×10^(-4)	1.5556×10^(-4)

Table 6. Total CPU Time for the IRK5, RK4, and CN Methods With $\Delta t = 0.1$, $\Delta x = 0.25$, $\alpha = \beta = \gamma = 1$, *and*v= 1.5

Method	iRK-5	RK-4	C-N
CPU time	0.07300 s	0.051046 s	0.075122 s

the values recorded in Table 5. While the Crank-Nicolson error in Figure 2c grows aggressively toward 1.2×10^{-3} as t approaches 1.0, the iRK-5 and RK-4 methods exhibit much more controlled growth, staying within the 10^{-4} range. Finally, the convergence of all error values at $\Delta t = 0.01$ across all three tables suggests that the numerical solution has reached a spatial bottleneck, where the total error is dominated by the grid size

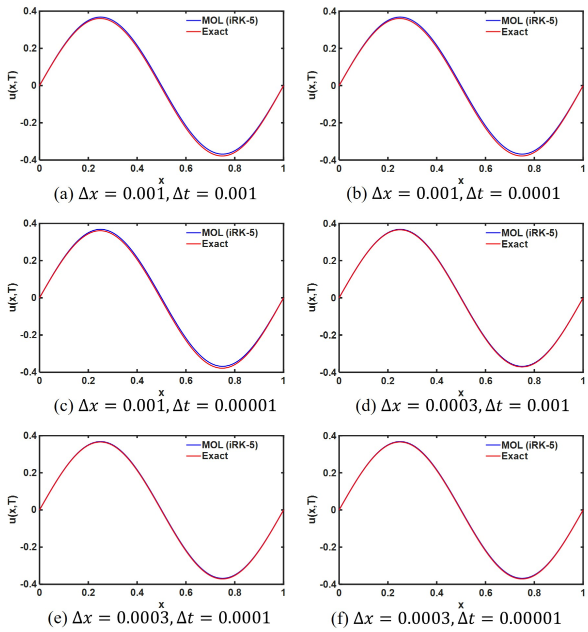

(a) $\Delta x = 0.001, \Delta t = 0.001$ (b) $\Delta x = 0.001, \Delta t = 0.0001$ (c) $\Delta x = 0.001, \Delta t = 0.00001$ (d) $\Delta x = 0.0003, \Delta t = 0.001$ (e) $\Delta x = 0.0003, \Delta t = 0.0001$ (f) $\Delta x = 0.0003, \Delta t = 0.00001$

Figure 4. Comparison of the Exact and Numerical Solutions of the KdV-BBM Equation (30) for $\beta = 1$, $\alpha = 1$, and $\gamma = 1$, with Various Values of Δx and Δt.

Δx. Regarding computational efficiency, Table 6 compares the total CPU time required by each scheme at $\Delta t = 0.1$. Although the RK-4 method achieves the shortest runtime of 0.051046" s" due to fewer stage evaluations, the iRK-5 method (0.07300" s") demonstrates better computational economy than Crank-Nicolson (0.075122" s"). Given that iRK-5 delivers superior accuracy at larger time steps, this marginal CPU overhead is offset by its ability to achieve high precision with larger steps, proving its overall computational superiority.

3.4 Numerical Simulation of the Homogeneous KdV-BBM Equation Using Method of Lines Scheme

Consider the KdV–BBM equation (30) subject to the given initial (31) and boundary conditions. To account for the periodic nature of the domain, the boundary conditions are incorporated by defining fictitious points such that $u_0 = u_M, u_{-1} = u_{M-1}, u_{M+1} = u_1$ and $u_{M+2} = u_2$. These relations ensure that the spatial derivatives at the boundaries are consistently approximated using the same central finite-difference scheme applied to the interior points. Consequently, the matrix A takes a circulant tridiagonal form, where the non-zero elements at the top-right and bottom-left corners represent the periodic coupling between the first and last grid points. This structure, combined with the inhomogeneous source term $\Delta x^2 g_j(t)$ in the vector $\vec{F}$, transforms the partial differential equation into a closed system of ordinary differential equations (ODEs) that preserves the conservation properties of the periodic wave. Consequently, the resulting system of ODEs can be written as follows.

$$A\frac{d\vec{u}}{dt} = \vec{F}(\vec{u}, t).$$

where

$$\vec{u}(t) = \begin{bmatrix} u_2(t) \\ u_3(t) \\ \vdots \\ u_{M-2}(t) \\ u_{M-1}(t) \end{bmatrix},$$

and

$$A = \begin{bmatrix} \Delta x^2 + \gamma & -\gamma & 0 & \cdots & 0 \\ -\gamma & \Delta x^2 + \gamma & -\gamma & \cdots & 0 \\ \vdots & \vdots & \ddots & \ddots & \vdots \\ 0 & \cdots & -\gamma & \Delta x^2 + \gamma & -\gamma \\ 0 & \cdots & 0 & -\gamma & \Delta x^2 + \gamma \end{bmatrix}.$$

and the right-hand side vector $\vec{F}(\vec{u}, t) = (F_1, \ldots, F_M)^T$, whose components are given by:

$$\begin{aligned} F_j(\vec{u}, t) = & -\frac{\Delta x}{2}\left(u_{j+1} - u_{j-1}\right) \\ & - \frac{1}{2\Delta x}\left(u_{j+2} - 2u_{j+1} + 2u_{j-1} - u_{j-2}\right) \\ & - \frac{\Delta x}{2} u_j \left(u_{j+1} - u_{j-1}\right) \\ & + \Delta x^2 g_j(t). \end{aligned}$$

The final system can be written as

$$\frac{d\vec{u}}{dt} = A^{-1}\vec{F}(\vec{u}, t).$$

Table 7. Numerical Error Metrics for Various Values Of Δx With $\Delta t = 0.001$ In Solving the KdV-BBM Equation (30)

Δx	E_K	E_R	E_RMSE
0.01	3.34 ×10^(-1)	7.77×10^(-2)	7.47×10^(-3)
0.002	6.62 ×10^(-2)	1.55×10^(-2)	2.96 ×10^(-4)
0.001	3.30×10^(-2)	7.75×10^(-3)	7.38×10^(-5)
0.0005	1.65×10^(-2)	3.87×10^(-3)	1.84×10^(-5)
0.0004	1.32×10^(-2)	3.10×10^(-3)	1.18×10^(-5)
0.0003	1.10×10^(-2)	2.58×10^(-3)	8.170×10^(-7)

The visualization in Figure 3 illustrates the comparison between the exact solution via the Differential Transform Method (DTM) and the Method of Lines (MOL) numerical solution with the iRK-5 scheme, confirming that decreasing the Δx value consistently improves accuracy until the numerical solution perfectly coincides with the exact values. The data in Table 7 validates this trend, where reducing Δx from 0.01 to 0.0003 results in a drastic decline in Mean Square Error (MSE) from

Table 8. Numerical Error Metrics for Various Values Of Δx And Δt In Solving the KdV-BBM Equation (30)

Δx	Δt	E_K	E_R	E_{RMSE}
1.00×10^(-3)	3.00×10^(-3)	3.29×10^(-2)	7.73×10^(-3)	7.34×10^(-5)
	1.00×10^(-3)	3.30×10^(-2)	7.75×10^(-3)	7.38×10^(-5)
	1.00×10^(-4)	3.30×10^(-2)	7.76×10^(-3)	7.38×10^(-5)
	1.00×10^(-5)	3.30×10^(-2)	7.76×10^(-3)	7.38×10^(-5)
3.00×10^(-4)	1.00×10^(-3)	1.10×10^(-2)	2.58×10^(-3)	8.17×10^(-6)
	1.00×10^(-4)	1.10×10^(-2)	2.59×10^(-3)	8.19×10^(-6)
	1.00×10^(-5)	1.10×10^(-2)	2.59×10^(-3)	8.19×10^(-6)

the order of 10^{-3} to 10^{-7}. This proves that variations in Δx exert a much more significant impact on solution quality than changes in Δt, as truncation errors in high-order Runge-Kutta methods are dominated by spatial discretization. Consequently, a finer grid resolution (such as $\Delta x = 0.0003$) is the primary key to capturing KdV-BBM wave dynamics without significant amplitude or phase deviations; while also correcting the misconception that larger Δx values could yield accurate results.

From the perspective of Von Neumann stability, selecting the parameter $\Delta t = 0.001$ is a crucial step that positions the entire spectrum of purely imaginary eigenvalues, $\lambda(\xi)$, within the absolute stability region of the iRK-5 method. The stability analysis indicates that the semi-discrete system is neutrally stable; thus, employing a sufficiently small Δt serves as a safe bound to prevent unstable numerical oscillations triggered by the dispersive terms β and γ. Simulation results confirm that by maintaining $\Delta t = 0.001$ and refining Δx, the scheme successfully minimizes numerical dissipative and dispersive effects. This demonstrates that the chosen Δt operational limit fully satisfies the stability criteria, allowing the generated wave profiles to precisely represent the exact solution without numerical phase lag, as demonstrated in the progression from 3a to Figure 3f.

Numerical simulation results for the KdV-BBM equation, as presented in Table 8, demonstrate that the scheme's accuracy is heavily dominated by spatial resolution (Δx) rather than the time step size (Δt). It is observed that reducing Δt from 10^{-3} to 10^{-5} while keeping Δx constant does not yield significant changes in error metrics; for instance, at $\Delta x = 0.001$, the MSE remains stable at the 10^{-5} order. Conversely, transitioning Δx from 0.001 to 0.0003 successfully reduces the MSE substantially to 8.17×10^{-6}. This phenomenon is visually validated in Figure 4, where the MOL (iRK-5) numerical solution curves and the DTM exact solution curves exhibit increasingly consistent convergence as the spatial grid is refined, regardless of the time step variations employed.

These characteristics align with the Von Neumann stability analysis, where the use of a high-order iRK-5 scheme ensures that as long as Δt remains within the bounds of the imaginary stability region, the temporal discretization error will be significantly smaller than the spatial error from the centered difference scheme. In terms of numerical stability bounds, the maximum stable time step size observed for this configuration is$\Delta t = 3.00 \times 10^{-3}$. Exceeding this threshold (for instance, set to $\Delta t \geq 4.00 \times 110^{-3}$) causes the numerical scheme to exceed its stability boundary, resulting in severe numerical instability and overflow errors (producing NaN values). Provided that $\Delta t \leq 3.00\times10^{-3}$, the scheme's stability remains well-preserved across all parameter configurations, showing no numerical oscillations that would degrade the wave profile. This confirms that to achieve optimal computational efficiency in solving the KdV-BBM equation, priority should be given to using a finer spatial grid, given that the model's sensitivity to Δx is far higher than its sensitivity to Δt within the stable range.

In the spatial convergence test (Table 9), conducted by controlling a sufficiently small fixed time step Δt, all three methods, iRK-5, RK4, and CN demonstrate a consistent spatial accuracy rate, with the spatial convergence order maintaining a value of approximately ≈ 2.00. As shown in Table 8, refining the spatial grid size from N = 50 ($\Delta x = 2.00 \times 10^{-2}$) to $N = 400(\Delta x = 2.50 \times 10^{-3})$ systematically reduces the E_∞ error from the order of 10^{-3} down to 10^{-5}. These numerical findings align perfectly with theoretical expectations, as the spatial derivatives of the KdV-BBM equation were discretized using a second-order central finite difference scheme $O(\Delta x^2)$.

In the temporal convergence test with $N = 200$ (Table 10), the total error for the RK4 and CN methods experiences immediate saturation (stagnation) at 1.6244×10^{-4} starting from $\Delta t = 2.00 \times 10^{-3}$. Consequently, the computed temporal convergence order yields zero. As highlighted in Table 2, this phenomenon stems from an order imbalance between the high-order temporal integrator and the second-order spatial discretization. Mathematically, the combined global error is expressed as:

$$\text{Total Error} = C_x(\Delta x)^2 + C_t(\Delta t)^p.$$

Because the spatial discretization error $O(\Delta x^2) \approx 1.62 \times 10^{-4}$ is significantly larger than the local temporal errors of RK4 ($O(\Delta t^4)$) and iRK-5 ($O(\Delta t^5)$), further reducing Δt no longer diminishes the total simulation error. Instead, the total error hits a lower threshold known as the spatial error floor.

Despite the temporal testing being constrained by the spatial error floor, the iRK-5 method still demonstrates dynamic superiority. As observed in Table 10, while the errors of RK4 and CN become entirely locked and show no response to decreasing Δt, the error of iRK-5 continues to progressively decrease from 2.5018×10^{-4} down to 1.7341×10^{-4}.This continuous reduction confirms that the iRK-5 scheme possesses higher numerical flexibility, enhanced stability, and superior temporal precision in approaching the spatial convergence limit compared to RK4 and CN.

3.5 Stability Analysis of the Numerical Scheme

In this section, the stability properties of the numerical scheme obtained through the method of lines (MOL) for the spatially discretized KdV-BBM equation are analyzed. The resulting semi-discrete system is subsequently integrated in time using the fifth-order improved Runge-Kutta method (iRK-5). The

Table 9. Spatial Convergence Analysis for the KdV-BBM Equation at $T = 1.0$ With Fixed $\Delta t = 5.00 \times 10^{-5}$

Δx	E_∞ (iRK-5)	Order	E_∞ (RK-4)	Order	E_∞ (C-N)	Order
2.00×10^{-2}	2.6143×10^{-3}	-	2.6132×10^{-3}	-	2.6132×10^{-3}	-
1.00×10^{-2}	6.5174×10^{-4}	2.00	6.5064×10^{-4}	2.01	6.5064×10^{-4}	2.01
5.00×10^{-3}	1.6354×10^{-4}	1.99	1.6244×10^{-4}	2.00	1.6244×10^{-4}	2.00
2.50×10^{-3}	4.1694×10^{-5}	1.97	4.0599×10^{-5}	2.00	4.0599×10^{-5}	2.00

Table 10. Temporal Convergence Analysis for the KdV-BBM Equation at T = 1.0 With Fixed N = 200 And $\Delta x = 5.00 \times 10^{-3}$

Δt	E_∞ (iRK-5)	Order	E_∞ (RK4)	Order	E_∞ (CN)	Order
4.00×10^(-3)	2.5018×10^(-4)	-	1.6244×10^(-4)	-	1.6503×10^(-4)	-
2.00×10^(-3)	2.0630×10^(-4)	0.28	1.6244×10^(-4)	-0.00	1.6309×10^(-4)	0.02
1.00×10^(-3)	1.8438×10^(-4)	0.16	1.6244×10^(-4)	-0.00	1.6260×10^(-4)	0.00
5.00×10^(-4)	1.7341×10^(-4)	0.09	1.6244×10^(-4)	-0.00	1.6248×10^(-4)	0.00

stability assessment is based on the classical Von Neumann (Fourier) analysis, in which the scheme is first linearized and boundary effects are neglected by assuming an infinite uniform grid.

The spatial discretization using centered finite differences yields the semi-discrete form:

$$\begin{aligned}\frac{du_j}{dt} &= -\frac{u_{j+1} - u_{j-1}}{2\Delta x} \\ &\quad + \gamma \frac{d}{dt}\left(\frac{u_{j+1} - 2u_j + u_{j-1}}{\Delta x^2}\right) \\ &\quad - \beta \frac{u_{j+2} - 2u_{j+1} + 2u_{j-1} - u_{j-2}}{2\Delta x^3} \\ &\quad - \alpha u_j \left(\frac{u_{j+1} - u_{j-1}}{2\Delta x}\right).\end{aligned}$$

To apply the Von Neumann analysis, the nonlinear term $(\alpha u_j u_x)$ is linearized by freezing the solution at a constant value U_0, resulting in the linear semi-discrete formulation.

$$\begin{aligned}\frac{du_j}{dt} &= -(1 + \alpha U_0)\,\delta_x u_j - \beta\,\delta_{xxx} u_j \\ &\quad + \gamma \frac{d}{dt}\left(\delta_{xx} u_j\right),\end{aligned}$$

which can be rewritten compactly as:

$$(1 - \gamma \delta_{xx})\, u_t = -\left[(1 + \alpha U_0)\delta_x + \beta\,\delta_{xxx}\right] u.$$

Assuming a Fourier mode solution:

$$u_j(t) = \hat{u}(t) e^{ij\xi}, \qquad \xi \in [0, \pi].$$

and substituting the corresponding operator symbols into the semi-discrete equation yields the eigenvalue:

$$\frac{\left[(1 + \alpha U_0)\Delta x^2 + 2\beta(\cos\xi - 1)\right]\sin\xi}{\Delta x\left[\Delta x^2 - 2\gamma(\cos\xi - 1)\right]}.$$

Since $\lambda(\xi) = i\omega(\xi)$ is purely imaginary for all $\xi \in [0, \pi]$, the semi-discrete system is neutrally stable in the continuous-time sense, i.e., no exponential growth occurs prior to time discretization.

After spatial discretization, the KdV-BBM system can be written as:

$$\frac{du}{dt} = Lu,$$

where L is the discrete spatial operator with eigenvalues $\lambda(\xi)$. Applying a one-step Runge-Kutta method to the scalar test equation.

$$\widehat{u}' = \lambda \widehat{u}$$

leads to the amplification relation

$$\widehat{u}^{n+1} = R(z)\widehat{u}^n, \qquad z = \Delta t\,\lambda,$$

with $R(z)$ denoting the stability function. The Von Neumann stability requirement for the fully discrete scheme is:

$$|R\left(\Delta t\,\lambda(\xi)\right)| \leq 1, \qquad \forall \xi \in [0, \pi].$$

Applying the iRK-5 method to the test equation gives stability.

$$R_5(z) = 1 + z + \frac{z^2}{2} + \frac{z^3}{6} + \frac{z^4}{24} + \frac{z^5}{120}.$$

Similar to RK-4, the method is conditionally stable for purely imaginary eigenvalues, and the CFL condition becomes:

$$\Delta t \leq \frac{z_5}{\max\limits_{\xi \in [0,\pi]} |\lambda(\xi)|},$$

where $z_5 > 0$ denotes the imaginary-axis stability limit.

In practice, the absolute stability region can be visualized in the complex plane to determine admissible values of$z =$

Table 11. Comparison of Numerical Methods for the KdV-BBM Equation

Method	Type of Approach	Order or Accuracy	Target Model Features	Main Advantages	Key Limitations
MOL (iRK-5)	Semi-discrete (Method of Lines)	High temporal accuracy $O(\Delta t^5)$, spatial accuracy $O(\Delta x^2)$	Homogeneous and inhomogeneous KdV-BBM	Superior stability, lower execution time, and high accuracy with larger time-step sizes	Requires ODE system integration
DTM	Analytical / Series Transformation	Arbitrary series convergence	Homogeneous and inhomogeneous KdV-BBM (Cauchy / periodic BCs)	Closed-form approximations without spatial/temporal discretization grids	Truncation order limits long-term temporal validity
Standard RK-4 / Finite Difference	Fully discrete	$O(\Delta t^4)$, $O(\Delta x^2)$	Homogeneous KdV-BBM	Simple implementation and well-known baseline	Strict CFL stability limits and requires very small Δt
Crank–Nicolson (C-N)	Implicit finite difference	$O(\Delta t^2)$, $O(\Delta x^2)$	Homogeneous KdV-BBM	Unconditionally stable	Low temporal accuracy order ($O(\Delta t^2)$) and requires large matrix inversions

$\Delta t\, \lambda(\xi)$. Therefore, for a given spatial discretization, the time step Δt must be chosen such that all Fourier modes remain within the stability region, ensuring the stability of the fully discrete KdV-BBM scheme.

To contextualize the advantages of the proposed dual computational strategy, a comparative evaluation against established numerical schemes for the KdV-BBM equation is summarized in Table 11 Standard explicit methods (such as RK-4) are bounded by strict Courant-Friedrichs-Lewy (CFL) stability constraints that demand excessively small time steps, while classical implicit schemes (such as Crank-Nicolson) exhibit lower second-order temporal accuracy (O(Δt^2)) and high computational costs due to repeated matrix inversions. In contrast, the proposed MOL(iRK-5) scheme addresses these limitations by achieving higher fifth-order temporal precision (O(Δt^5)) alongside an expanded stability domain along the imaginary axis. This elevated temporal accuracy allows the numerical solver to operate efficiently with larger time steps (e.g., Δt^2 = 0.5) while maintaining superior numerical stability, preserving physical solitary wave characteristics (soliton peak height and phase speed), and maintaining lower overall CPU execution times compared to conventional solvers. Simultaneously, the DTM semi-analytical framework provides an exact, meshless reference solution, making this combined investigation a comprehensive computational benchmark for non-local dispersive wave equations.

A rigorous evaluation of Tables 3, 4, and 5 reveals that while the global error magnitudes of iRK-5 and RK-4 appear closely matched under refined time steps, iRK-5 consistently yields smaller residual errors across all metrics ($E_\infty, E_R, andE_K$). Furthermore, the temporal convergence analysis in Table 10 provides crucial insight into the dynamic order behavior of both schemes. Although neither method reaches its theoretical temporal order (O(Δt^5) for iRK-5 and O(Δt^4) for RK-4) due to spatial error contamination from the second-order finite difference scheme (O(Δx^2) floor at $\approx 1.62 \times 10^{-4}$), iRK-5 exhibits a distinctly higher effective convergence order than RK-4. As Δt is refined from 4.00×10^{-3} to 5.00×10^{-4}, the errors for RK-4 immediately saturate and lock at 1.6244×10^{-4} (yielding a calculated order of 0.00), whereas the error for iRK-5 continues to decrease progressively from 2.5018×10^{-4} down to 1.7341×10^{-4} (maintaining non-zero order values). This persistent reduction confirms that iRK-5 possesses superior temporal precision, enhanced stability, and higher numerical flexibility in penetrating the spatial error floor compared to RK-4 and Crank-Nicolson schemes.

4. CONCLUSIONS

This study advances the computational treatment of nonlinear dispersive wave dynamics by establishing a robust dual framework encompassing both semi-analytical and numerical approaches for solving the KdV-BBM equation. The primary scientific contribution lies in demonstrating how the Differential Transformation Method (DTM) can be adapted via Cauchy boundary conditions for homogeneous systems and Nayar's Theorem for inhomogeneous configurations to construct exact series solutions that serve as rigorous mathematical benchmarks. Complementary to this, the Method of Lines integrated with an improved fifth-order Runge-Kutta solver (MOL-iRK-5) successfully addresses long-term spatio-temporal simulation demands: it offers superior phase preservation, effectively suppresses amplitude dissipation, and achieves strong numerical stability without the heavy matrix inversion costs associated with implicit solvers. Despite these contributions, the proposed computational strategies exhibit specific limitations that highlight avenues for future development. Notably, although the temporal integrator is theoretically designed as a fifth-order scheme (O(Δt^5)), the overall observed global numerical accuracy does not fully attain fifth-order precision in practice. This reduction in the effective global convergence rate is primarily driven by the spatial discretization bottleneck, where the lower second-order spatial finite difference operator (O(Δx^2))

dominates the global error profile, combined with numerical stiff-decay and boundary error propagation inherent in nonlinear dispersive PDEs. Additionally, the semi-analytical DTM power series is subject to a finite radius of convergence, limiting its direct applicability over long time horizons without implementing domain decomposition techniques. Finally, because the current MOL formulation relies on uniform spatial grids, extending this approach to irregular geometries or adaptive mesh structures will require further mathematical reformulation of the discrete operator matrices.

5. ACKNOWLEDGEMENT

The authors would like to express their gratitude to the UB STARS research program at Universitas Brawijaya and the National Research and Innovation Agency (BRIN) for providing the necessary facilities and technical support that made this research possible. This work was supported by the Brawijaya University under Grant No: 06872.4/UN10.F0901/B/PT/2025.

REFERENCES

Alshareef, A. and H. Bakodah (2025). Non-Central M-Point Formula in Method of Lines for Solving the Korteweg-de Vries (KdV) Equation. *Journal of Umm Al-Qura University for Applied Sciences*, **11**(1); 142–152

Aris Izzuddin Razali, M. and N. Azliza Abd Latif (2022). Solving Lane-Emden Equation by Using Differential Transformation Method. In *International Conference on Educational Technology and Administration*. Springer, pages 3–13

Ayaz, F. (2004). Solutions of the System of Differential Equations by Differential Transform Method. *Applied Mathematics and Computation*, **147**(2); 547–567

Babayar-Razlighi, B. and B. Soltanalizadeh (2022). Application of Differential Transformation Method to the Dullin-Gottwald-Holm Equation. *Mathematical Analysis and Convex Optimization*, **3**(1); 23–35

Brociek, R. and M. Pleszczyński (2024). Differential Transform Method and Neural Network for Solving Variational Calculus Problems. *Mathematics*, **12**(14); 2182

Carvajal, X. and M. Panthee (2022). On Propagation of Regularities and Evolution of Radius of Analyticity in the Solution of the Fifth-Order KdV–BBMModel: X. Carvajal and M. Panthee. *Zeitschrift für angewandte Mathematik und Physik*, **73**(2); 68

Cheng, Y. and Y. Li (2026). Partial Differential Equation (PDE)-Based Spatial Pharmacometrics in NONMEM: Method of Lines (MOL) Implementation with AI-Assisted Model Development. *The Journal of Clinical Pharmacology*, **66**(6); e70215

Faishal, M. A. and M. K. Hasan (2025). A More Efficient Differential Transform Method for Solving Relativistic Equation. *Noise & Vibration Worldwide*; 09574565261459697

Gao, D., Z. Qiu, L. Wang, and J. Li (2025). Crank–Nicolson Quasicompact Schemes for One-Sided Tempered Fractional Diffusion Equations (without Using Points Outside the Interval). *Boundary Value Problems*, **2025**(1); 52

Habibah, U., F. F. Medrano, A. C. Permana, D. Ardiana, et al. (2025a). An Improved Fifth-Order Runge-Kutta Method with Higher Accuracy and Efficiency for Solving Initial Value Problems. *Science and Technology Indonesia*, **10**(3); 802–816

Habibah, U., Z. C. Rohman, Y. N. Dewanti, and A. N. Hananti (2025b). Analytical and Numerical Solutions of the Convection-Diffusion-Reaction Equations Applying the Differential Transformation Method and the Crank-Nicholson Method along with Stability Analysis and Truncation Error Analysis. *Computational Methods for Differential Equations*

Hossain, A. K. S., M. A. Akbar, and M. I. Hossain (2025). Modified Simple Equation Technique for First-Extended Fifth-Order Nonlinear Equation, Medium Equal Width Equation and Caudrey–Dodd–Gibbon Equation. *Journal of Umm Al-Qura University for Applied Sciences*, **11**(3); 623–632

Khatun, M. M. and M. A. Akbar (2024). Analytical soliton solutions of the beta time-fractional simplified modified Camassa-Holm equation in shallow water wave propagation. *Journal of Umm Al-Qura University for Applied Sciences*, **10**(1); 120–128

Liu, K., Z. Liu, and H. Zhao (2024). Exponential Stability of the Linear KdV-BBM Equation. *Discrete and Continuous Dynamical Systems-Series B*, **29**(3); 1206–1216

Mebrate, S., T. Dufera, and A. Tesfahun (2024). Improved Lower Bound for the Radius of Analyticity of Solutions to the Fifth Order, KdV-BBM Type Equation. *Bulletin of the Iranian Mathematical Society*, **50**(4); 62

Meyer, G. H. (1978). The Method of Lines for Poisson's Equation with Nonlinear or Free Boundary Conditions. *Numerische Mathematik*, **29**(3); 329–344

Muhammad, K. A., A. A. Isa, T. Sarita, and S. M. D. Voumo (2025). Application of Reduced Differential Transform Method to Solve Linear, Non-Linear Convection-Diffusion and Reaction-Diffusion Problems. *MSI Journal of Multidisciplinary Research (MSIJMR)*, **2**(5); 55–64

Nayar, H. and P. A. Phiri (1974). The Fornberg-Whitham Equation Solved by the Differential Transform Method

Nolasco Serna, C., N. Afanador García, and G. Guerrero Gómez (2022). Aplicaciones Del álgebra Lineal Al Estudio Del Modelado Matemático De Los Fenómenos Físicos De Conducción De Calor Por Electricidad

Odibat, Z. M. (2008). Differential Transform Method for Solving Volterra Integral Equation with Separable Kernels. *Mathematical and Computer Modelling*, **48**(7-8); 1144–1149

Pava, J. A. (2018). Stability Properties of Solitary Waves for Fractional KdV and BBM Equations. *Nonlinearity*, **31**(3); 920–956

Polwang, A., K. Poochinapan, and B. Wongsaijai (2025). Numerical Simulation of Wave Flow: Integrating the BBM-KdV Equation Using Compact Difference Schemes. *Mathematics and Computers in Simulation*, **236**; 70–89

Putri, D. P. N. and U. Habibah (2026). Numerical Solution of the Gardner Equation Using the Method of Lines and an

Improved Fifth-Order Runge-Kutta Scheme. *Science and Technology Indonesia*, **11**(3); 903–914

Qin, Y. and Q. Lou (2021). Differential Transform Method for the Solutions to Some Initial Value Problems in Chemistry. *Journal of Mathematical Chemistry*, **59**(4); 1046–1053

Ramli, M., D. Irsalina, I. P. Iwanisa, and V. Halfiani (2017). Soliton Solution of Benjamin-Bona-Mahony Equation and Modified Regularized Long Wave Equation. In *AIP Conference Proceedings*, volume 1913. AIP Publishing LLC, page 020002

Saha Ray, S. et al. (2020). Invariant Analysis, Optimal System of Lie Sub-Algebra and Conservation Laws of (3+ 1)-Dimensional KdV–BBM Equation. *The European Physical Journal Plus*, **135**(11); 913

Sarker, S., R. Karim, M. A. Akbar, M. Osman, and P. Dey (2024). Soliton Solutions to a Nonlinear Wave Equation Via Modern Methods. *Journal of Umm Al-Qura University for Applied Sciences*, **10**(4); 785–792

Suebcharoen, T., K. Poochinapan, and B. Wongsaijai (2022). Bifurcation Analysis and Numerical Study of Wave Solution for Initial-Boundary Value Problem of the KdV-BBM Equation. *Mathematics*, **10**(20); 3825

Sweilam, N., N. B. E. Din, M. Ammar, and E. Abo-Eldahab (2025). Compact Finite Difference Schemes with Spectral-Like Resolution for Solving Nonlinear Heat-Wave Propagation in a Rigid Thermal Conductor. *Journal of Umm Al-Qura University for Applied Sciences*; 1–16

Tegegn, E., A. Tesfahun, and B. Belayneh (2023). Lower Bounds on the Radius of Spatial Analyticity of Solution for KdV-BBM Type Equations: E. Tegegn, A. Tesfahun and B. Belayneh. *Nonlinear Differential Equations and Applications NoDEA*, **30**(4); 47

Verwer, J. G. and J. M. Sanz-Serna (1984). Convergence of Method of Lines Approximations to Partial Differential Equations. *Computing*, **33**(3); 297–313

Voigt, A. (1979). The Method of Lines for Nonlinear Parabolic Differential Equations with Mixed Derivatives. *Numerische Mathematik*, **32**(2); 197–207

Wang, J., H. Li, X. Ren, and X. Chang (2025). The Crank-Nicolson Mixed Finite Element Scheme and Its Reduced-Order Extrapolation Model for the Fourth-Order Nonlinear Diffusion Equations with Temporal Fractional Derivative. *Fractal and Fractional*, **9**(12); 789

Zhou, J. (1986). Differential Transformation and Its Applications for Electrical Circuits. *Huazhong University Press, Wuhan China (In Chinese) google schola*, **2**; 413–420